OPTICAL REVIEW Vol. 7, No. 4 (2000) 297–302

Output Characteristics of High-Power Continuous Wave Raman Fiber Laser at 1239 nm Using Phosphosilicate Fiber

Mahendra PRABHU[1], Nam Seong KIM[1,2] and Ken-ichi UEDA[1]

[1]*Institute for Laser Science, University of Electro-Communications, 1-5-1 Chofugaoka, Chofu, Tokyo, 182-8585 Japan,*
[2]*Information and Telecommunication Technology Center, The University of Kansas, 2291 Irving Hill Road, Lawrence, Kansas, 66045 U.S.A*

(Received December 7, 1999; Accepted March 16, 2000)

A high-power singlemode Raman fiber laser (RFL) with maximum output power of 4.11 W and maximum power conversion efficiency of 47.40% at 1239 nm is realized using continuous wave 8.4 W Yb-doped double-clad fiber laser as a pump, 700 m phosphosilicate fiber, and a Raman cavity formed by a pair of fiber Bragg grating mirrors at 1239 nm. The output characteristics of the RFL at 1239 nm for different fiber lengths and output mirror reflectance are reported. Theoretical simulation is done to numerically optimize for fiber length and output coupler reflectivity to obtain maximum first Stokes power.

Key words: Raman fiber laser, phosphosilicate fiber, double-clad fiber laser, optical fiber, stimulated Raman scattering, fiber Bragg grating

1. Introduction

Raman amplifiers and lasers played a vital role in the field of optical communication in the early 1980s following their discovery in 1972.[1–31] However, with the advent of Er-doped fiber in the early 1990s, this has been used in fiber amplifiers and lasers in the 1550 nm wavelength low-loss optical window.[32,33] In the late 1990s, the high-power multimode 810 nm/915 nm/980 nm laser diodes and singlemode fiber lasers like ytterbium-doped double-clad fiber laser (DCFL) at 1064 nm re-stimulated research in Raman fiber lasers (RFL) and Raman fiber amplifiers (RFA).

The stimulated Raman scattering (SRS) in the RFL and the RFA involves a frequency-conversion process in which light traveling down a fiber interacts with the vibrating molecules in silica material. This interaction triggers a spectral shift that transfers the energy from a shorter-wavelength pump beam to a longer-wavelength signal one. Though the Raman gain can be obtained from any silicate fiber, the value of Raman gain coefficient is about eight times higher for germanosilicate fiber than that for silicate fiber; hence, the former is used extensively in RFL and RFA. Using the germanosilicate fiber with a peak Raman shift of 440–490 cm^{-1}, the third and the sixth Stokes orders produce outputs at 1240 nm and 1480 nm, respectively, with a 1060 nm pump source. However, the low-loss phosphosilicate (P_2O_5-SiO_2) fiber has a peak Raman shift of 1330 cm^{-1} as shown in Fig. 1; this is due to oxygen double-bonded to P atoms.[6] When it is pumped with a 1060 nm pump source, the first and second Stokes orders occur at 1240 nm and 1480 nm, respectively. Figure 2 and Table 1 show the loss spectrum and the fiber parameters of the phosphorous-doped fiber (PDF) which were used in the simulation and experiments. The PDF has a loss of 1.12 and 0.95 dB/km at 1240 and 1484 nm, respectively. The 12-mole% phosphorous concentration results in a refractive index difference of 0.0105. A high-power RFL can be obtained using PDF and low-loss, high-reflectivity fiber Bragg grating (FBG) mirrors.[34–36]

Along with the practical realization of RFL and RFA, there have also been many theoretical and numerical papers on optimization of RFL output. This involves solving the non-linear coupled differential equations using various numerical and analytical methods.[37–40]

The theoretical model used to analyze and optimize the RFL performance is discussed in Sect. 2. The set of non-linear coupled equations which describe the RFL are solved using both the linear shooting method and the finite difference method. The theoretical model used for the simulation is also detailed. The performances of the RFL for different fiber lengths and output coupler reflectivity are reported in Sect. 3, and the experimental setup and results in Sect. 4. In Sect. 5 we draw our conclusions.

2. Theoretical Model

The basic layout of the RFL is shown in Fig. 3. The pump source at 1064 nm is spliced to the Raman cavity, which consists of a pair of FBG mirrors. FBG1 has a reflectivity greater than 99% at 1239 nm, while the reflectivity of FBG2 is varied. Once the pump power is increased above the first Stokes threshold, the first Stokes order is generated in both forward and backward directions. The forward/backward Stokes orders propagate in their respective directions along the fiber and encounter the FBG at $z=0$ or L. Since the FBG has a low insertion loss and very narrow bandwidth of about 1 nm, it reflects only the selective wavelengths. Hence, the forward and backward first Stokes orders are reflected back into the cavity. A fraction of the first-Stokes power at the output coupler is coupled out as laser output from the out-

E-mail: prabhu@ils.uec.ac.jp

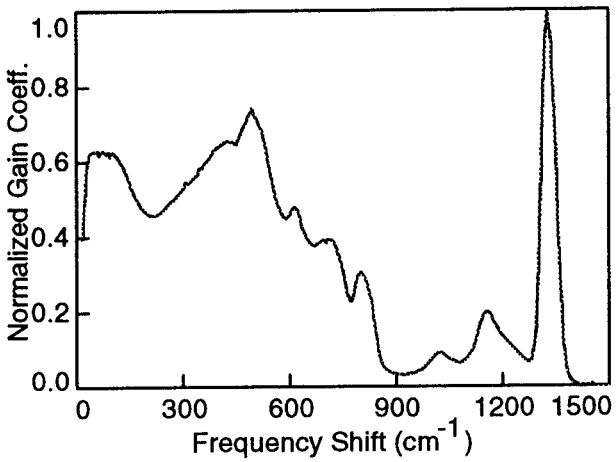

Fig. 1. Raman spectrum of phosphosilicate fiber.

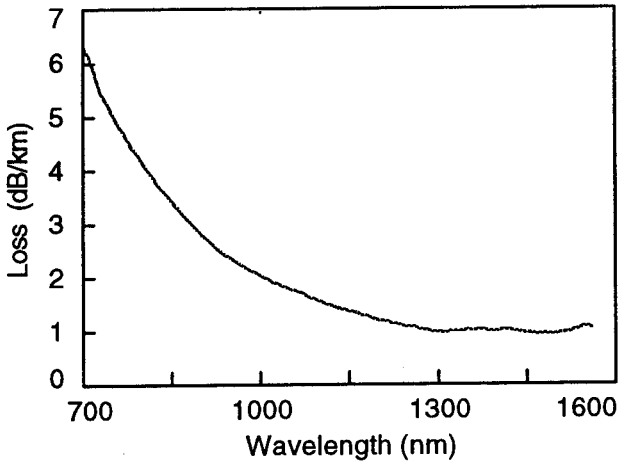

Fig. 2. Loss spectrum of phosphosilicate fiber.

Table 1. Fiber parameters of the phosphorous-doped fiber used in the simulation and the experiments.

Fiber parameter	Value
Fiber loss	
@1064 nm	1.77 dB/km
@1240 nm	1.12 dB/km
@1480 nm	0.95 dB/km
Core diameter	6.2 um
Fiber diameter	125 um
Cutoff wavelength	1.05 um
Refractive index difference	0.0105
Phosphorous concentration	12 mol%
Mode field diameter	
@1.064 um	5.96 um
@1.24 um	7.05 um
@1.48 um	8.25 um
Raman gain	
@1.24	5.4 dB/km/W
@1.48	4.5 dB/km/W

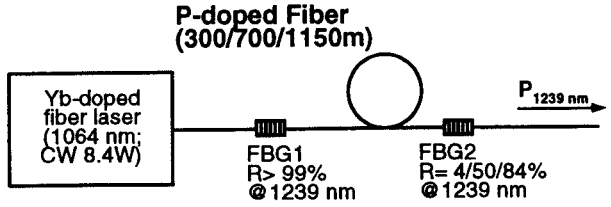

Fig. 3. Setup for the 1239 nm RFL pumped by CW 8.4 W Yb-doped double-clad fiber laser.

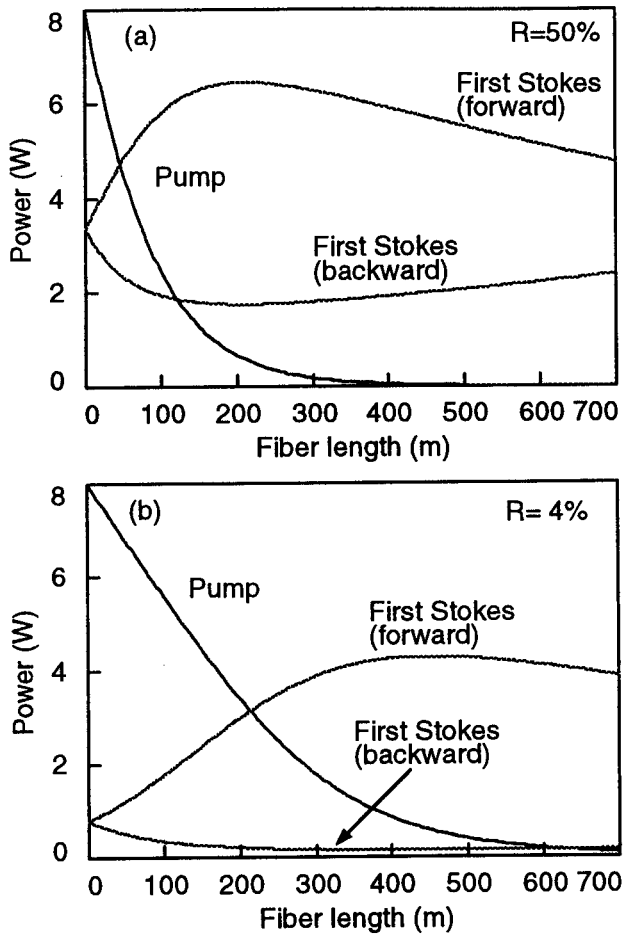

Fig. 4. Power evolution of forward/backward first Stokes powers and pump power versus PDF fiber length for two different output coupler reflectivities. (a) R=50%, (b) R=4%.

put end of the FBG mirror. The laser output depends on the output coupler reflectivity.

The steady-state RFL can be modeled using the nonlinear coupled differential equations as follows:

$$\frac{dP_P}{dz} = -\frac{g_R}{A}\left(\frac{\omega_p}{\omega_{S1}}\right)(P_{S1F}+P_{S1B})P_P - \alpha_P P_P$$

$$\frac{dP_{S1F}}{dz} = g_R P_{S1F} P_P - \alpha_{S1} P_{S1F}$$

$$\frac{dP_{S1B}}{dz} = -[g_R P_{S1B} P_P - \alpha_{S1} P_{S1B}], \quad (1)$$

where P_P, P_{S1F} and P_{S1B} are the pump, the forward first Stokes, and the backward first Stokes powers, respectively; g_R is Raman gain coefficient, α_P and α_{S1} are linear attenuation coefficients at the pump and the first Stokes wavelengths, respectively; A is the effective core area, and ω_P and ω_{S1} are the pump and the first Stokes frequencies, respectively.

To solve Eq. (1), we need to define the boundary conditions, as the RFL is a boundary value problem. The boundary conditions can be deduced from the output coupler reflectivities. By solving Eq. (1) using the linear shooting method or the finite difference method, we can determine the power evolutions along the fiber for the pump, the forward and the backward first Stokes orders.

Figure 4 (a) and (b) show the power evolution of the pump, the forward and the backward first Stokes orders for the RFL, which is configured at 1239 nm with 700 m phosphosilicate fiber, input FBG1 with high-reflectivity and output FBG2 mirrors with reflectivity of 50% and 4%, respectively. In our simulation, we have assumed the FBG1 to have a reflectivity of 100% at 1239 nm. Therefore, the forward first Stokes and the backward first Stokes powers match at $z=0$, whereas at $z=L$ the backward first Stokes power is determined by the product of the forward first Stokes power and the output coupler reflectivity.

Although the simulations were done for fiber length ranging from 0 to 1150 m, we focused mainly on fiber lengths of 300 m, 700 m, and 1150 m that were used in the experiments. Similarly, simulations for three output coupler reflectivities of 4%, 50%, and 84% were performed to match the experimental conditions.

3. Results of the Simulation

Theoretical simulation was done to optimize the RFL to achieve maximum first Stokes power by varying the fiber length and the output coupler reflectivity independently. Equation (1) was solved using the shooting and the finite difference method. The shooting method is used to solve ordinary differential equations that satisfy boundary conditions at more than one value of the independent variable. The above equation was solved with boundary conditions obtained by multiplication of the powers of the previous passage with mirror reflectivities at $z=0$ and L. The initial conditions were adjusted until a stable solution was obtained to match the values of the input pump power, the forward and the backward first Stokes powers to the boundary conditions.

The results of the simulation are summarized in Fig. 5. The power conversion efficiency and the first Stokes threshold are plotted as a function of the fiber length in Fig. 5(a) and (b). The power conversion efficiency (PCE$=P_{out}(\lambda 1239)/P_{in}(\lambda 1064)$) of 48.6% is obtained for $L=300$ m with output coupler reflectivity of $R=50\%$.

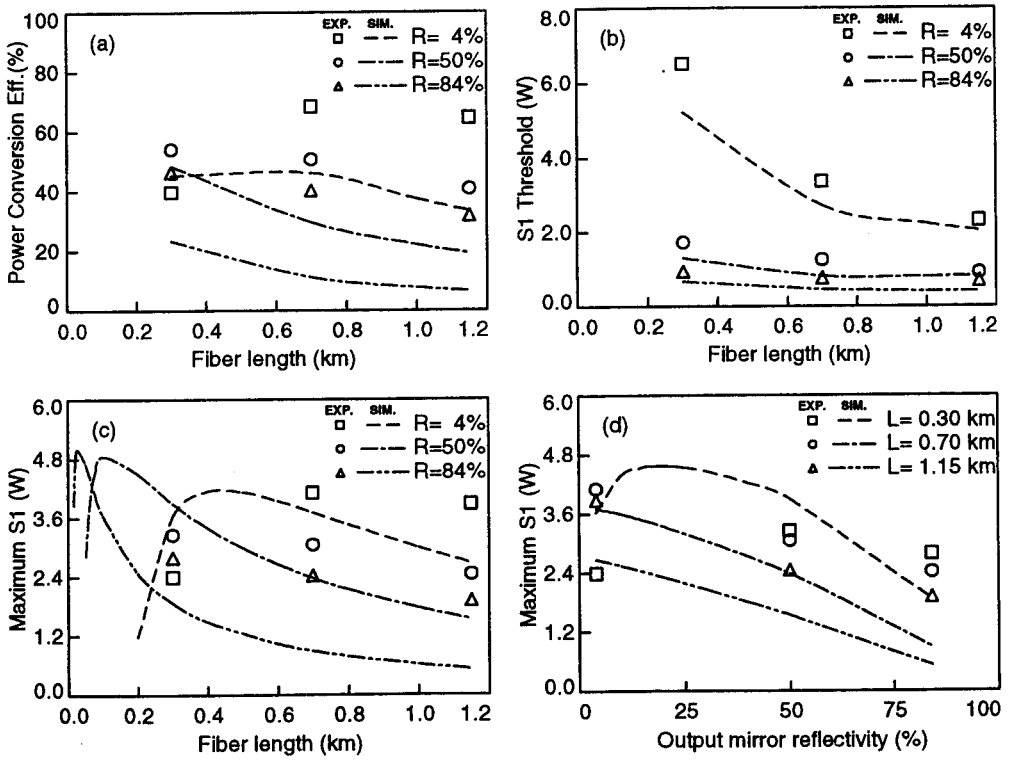

Fig. 5. Theoretical simulation and experimental results: The lines correspond to the theoretical simulations whereas the points represent the experimental data. (a) Variation of power conversion efficiency versus fiber length for different output coupler reflectivity. (b) Variation of first Stokes (S1) threshold versus fiber length for different output coupler reflectivity. (c) Variation of maximum first Stokes power versus fiber length for different output coupler reflectivity to optimize for fiber length. (d) Variation of maximum first Stokes power versus output mirror reflectivity for different fiber lengths to optimize for output coupler reflectivity.

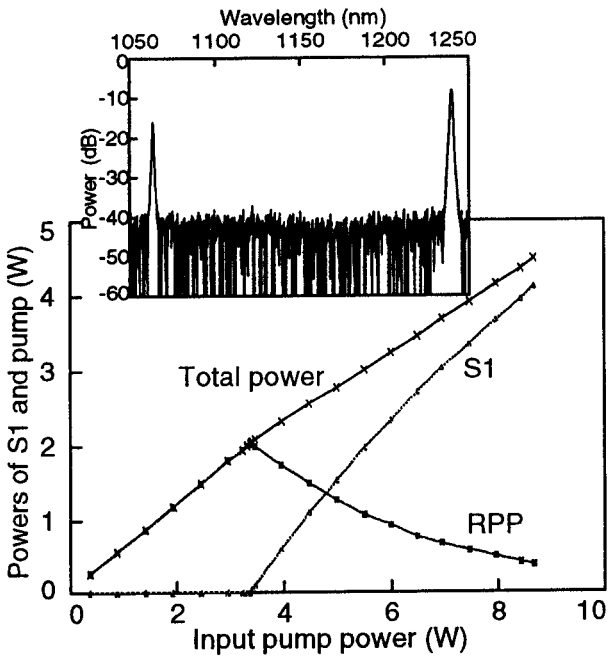

Fig. 6. Output powers of the residual pump and the first Stokes power with change in input pump power for 700 m of PDF and 4% output coupler reflectivity. Inset: output spectrum for 4.11 W first Stokes output.

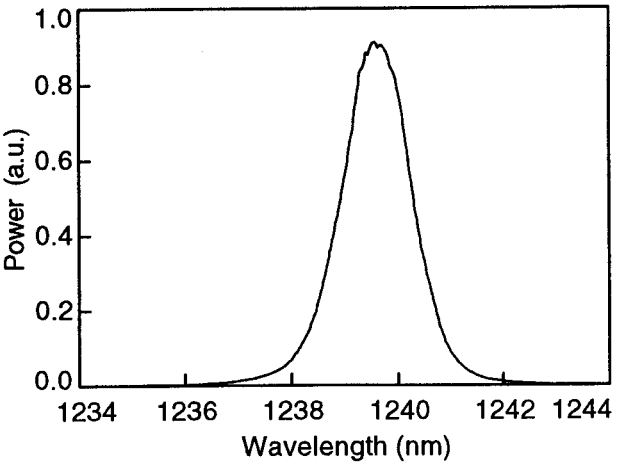

Fig. 7. Spectrum of the first Stokes output at 1239 nm for 700 m PDF length and 4% output coupler reflectivity.

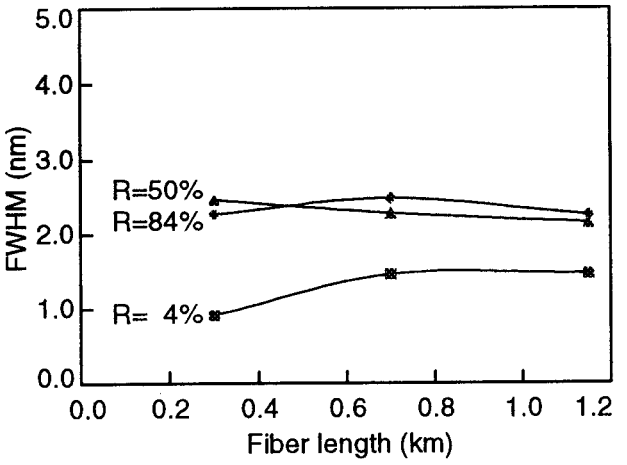

Fig. 8. Variation of the FWHM of the first Stokes output for different fiber length and output coupler reflectivity.

However, for 700 m PDF length and output coupler reflectivity of 4%, the PCE of 46.3% can be obtained. From Fig. 5(b), we understand that the threshold power decreases with increase in fiber length. Moreover, the RFL with output coupler reflectivity of 4% has the highest first Stokes threshold and PCE. In this case, the first Stokes power reflected from the output coupler and used in generation of the SRS is very small, and it results in an increased first Stokes threshold. In contrast, in the RFL with higher output coupler reflectivity, the first Stokes power reflected from the output coupler in the cavity is large and it results in decrease of the first Stokes threshold. In addition, only a smaller fraction of the first Stokes power is coupled out of the RFL cavity. In the RFL with the output FBG reflectivity of 4%, the first Stokes threshold is very high at 5.21 W.

In optimization of fiber length and output coupler reflectivity, both the PCE and the first Stokes threshold are important parameters. Figure 5(c) shows the variation of the maximum first Stokes power as a function of fiber length. The maximum first Stokes power of 4.99 W can be obtained for an RFL cavity with fiber length of 25 m and output coupler reflectivity of 84%. However, a large unabsorbed pump power at the fiber output is not desirable. As shown in Fig. 5(d), we can understand that for 19% output coupler reflectivity and 300 m fiber length, the maximum first Stokes power of 4.57 W can be obtained. For fiber lengths of 700 m and 1150 m, the maximum first Stokes power can be achieved for the output coupler with 4% reflectivity. After optimizing fiber length and output coupler reflectivity for maximum first Stokes power, we can obtain 4.61 W of first Stokes power with a fiber length of 250 m and output coupler reflectivity of 19%.

4. Experimental Results

The experimental setup for the RFL at 1239 nm is shown in Fig. 3. The pump source is the Yb-doped DCFL with singlemode fiber output and maximum output power of continuous wave (CW) 8.4 W at 1064 nm which was manufactured by IRE-Polus. The PDF and the FBGs were obtained from General Physics Institute, Russia. The Yb-doped DCFL has the output fiber of Flexcor-1060 and it was spliced with low loss to the Raman cavity, which consists of a pair of FBG mirrors written in the Flexcor-1060 fiber and the PDF. The mode-field diameters (MFD) of the PDF are 5.96 and 7.05 μm at 1064 nm and 1239 nm wavelengths, respectively, whereas the

corresponding MFD for the Flexcor-1060 are 6.16 μm and 7.13 μm, respectively. The mismatch in the MFD of the Flexcor-1060 and PDF results in a splicing loss between them, the average loss being 0.22 dB.

The output characteristics of the nine RFL cavities for the fiber lengths of 300 m, 700 m, and 1150 m and for the output coupler reflectivity of 4%, 50%, and 84% are reported. Figure 6 shows the variation of the first Stokes power and the residual pump power for change in the input pump power for 700 m PDF length and 4% output mirror reflectivity. For that RFL configuration, the laser threshold, the PCE efficiency, and the slope efficiency were 3.36 W, 47.40%, and 76.87%, respectively. The full width at half maximum (FWHM) is 1.46 nm and the first Stokes power at the output 4.11 W. The inset of Fig. 6 shows the output spectrum of the RFL, which includes the residual pump power and the first Stokes power. The spectrum was measured using an AQ-6315A optical spectrum analyzer by the ANDO Co. There was no silicate Stokes at 1120 nm as reported by Karpov *et al.*[36]

The consolidated results of the experiments are also shown in Fig. 5. Maximum PCE was achieved for the output coupler reflectivity of 4% and the 700 m PDF length. This result is very similar to the theoretical simulation wherein, for the 700 m PDF length, maximum first Stokes output occurred for 4% output coupler reflectivity.

The variation of the first Stokes threshold with respect to the fiber length as shown in Fig. 5 (b) is similar to the theoretical results. The RFL with 4% output coupler reflectivity has high first Stokes threshold and it decreases exponentially with increase in PDF length. Figure 5 (c) and (d) show the variation of first Stokes power as a function of the PDF length and the output mirror reflectivity. The maximum output from the RFL is obtained for the length of 700 m and 4% output coupler reflectivity. However, as shown in Fig. 5 (d), the output from the RFL with 300 m PDF length is much smaller than the theoretical calculations. This is ascribed to a large amount of residual pump power that has not been converted into the first Stokes power.

Figure 7 shows the output spectrum for the RFL with 700 m PDF length and 4% output coupler reflectivity. The spectral peak is at 1239.38 nm and the FWHM is 1.46 nm. Figure 8 shows the variation of the FWHM with change in PDF length and output coupler reflectivity. For 4% output coupler reflectivity, the FWHM is seen to be smaller compared to the 50% and 84% cases, where the first Stokes power inside the cavity is much larger; this results in increase of the FWHM.

5. Conclusions

We have performed theoretical simulations and the experiments to optimize the RFL performance for the PDF length and the output coupler reflectivity to achieve maximum PCE and first Stokes power.

The results of the simulation show that we can achieve a maximum first Stokes power of 4.61 W and PCE of 57.64% for 250 m PDF length and 19% output coupler reflectivity. The experiments for the RFL were performed for 300 m, 700 m, and 1150 m PDF lengths and 4%, 50%, and 84% of output coupler reflectivity. The maximum first Stokes power of 4.11 W and the PCE of 47.40% were achieved for the fiber length of 700 m and 4% output FBG reflectivity and are in good accordance with the theoretical simulation results.

The RFL at 1239 nm can be used as a pump source to amplify signals in the 1.31 μm wavelength band for optical fiber communications.

Acknowledgments

The authors acknowledge the financial support of the Japan Space Forum for this work. The PDF and the FBG mirrors used for the experiments were supplied by E. M. Dianov, V. M. Mashinsky, and S. A. Vasiliev at General Physics Institute, Russia. The Yb-doped fiber laser was supplied by IRE-Polus Inc.

References

1) R. H. Stolen, E. P. Ippen and A. R. Tynes: Appl. Phys. Lett. **20** (1972) 62.
2) R. G. Smith: Appl. Opt. **11** (1972) 2489.
3) C. Lin and R. H. Stolen: Appl. Phys. Lett. **29** (1976) 428.
4) K. O. Hill, D. C. Johnson and B. S. Kawasaki: Appl. Phys. Lett. **29** (1976)185.
5) B. S. Kawasaki, K. O. Hill and D. C. Johnson: Appl. Opt. **16** (1977) 1239.
6) F. L. Galeener, J. C. Mikkelsen, R. H. Geils and W. J. Mosby: Appl. Phys. Lett. **32** (1978) 34.
7) A. Y. J. Auyeung: IEEE J. Quantum Electron. **14** (1978) 347.
8) R. H. Stolen, C. Lin, J. Shah and R. F. Leheny: IEEE J. Quantum Electron. **14** (1978) 860.
9) R. H. Stolen: Proc. IEEE **68** (1980) 1232.
10) E. Brinkmeyer: J. Opt. Soc. Am. **70** (1980) 1010.
11) M. Ikeda: Opt. Commun. **39** (1981) 148.
12) Y. Kato, S. Seikai and M. Tateda: Appl. Opt. **21** (1982) 1332.
13) S. K. Y. Aoki, H. Honmou, K. Washio and M. Sugimoto: Electron. Lett. **19** (1983) 620.
14) E. Desurvire, M. Papuchon, J. P. Pocholle and J. Raffy: Electron. Lett. **19** (1983) 751.
15) R. H. Stolen, C. Lee and R. K. Jain: J. Opt. Soc. Am. B **1** (1984) 652.
16) M. Nakazawa, M. Tokuda, Y. Negishi and N. Uchida: J. Opt. Soc. Am. **1** (1984) 80.
17) N. Nakamura, M. Kimura, S. Yoshida, T. Hidaka and Y. Mitsuhashi: J. Lightwave Technol. **LT-2** (1984) 379.
18) M. L. Dakss and P. Melman: IEEE J. Lightwave Technol. **LT-3** (1985) 806.
19) J. Hegarty, N. A. Olsson and L. Goldner: Electron. Lett. **21** (1985) 290.
20) M. Nakazawa: Appl. Phys. Lett. **46** (1985) 728.
21) N. A. Olsson and J. Hegarty: IEEE J. Lightwave Technol. **LT-4** (1986) 396.
22) K. Ochizuki, N. Edagawa and Y. Iwamoto: IEEE J. Lightwave Technol. **LT-4** (1986) 1328.
23) K. Vilhelmsson: IEEE J. Lightwave Technol. **LT-4** (1986) 400.
24) E. Desurvire, A. Imamoglu and H. J. Shaw: IEEE J. Lightwave Technol. **LT-5** (1987) 89.
25) H. A. Haus and M. Nakazawa: J. Opt. Soc. Am. B **4** (1987) 652.
26) K. Suzuki and M. Nakazawa: Opt. Lett. **13** (1988) 666.
27) F. Irrera, L. Lamberto and D. Pozza: J. Appl. Phys. **63** (1988) 2882.

28) A. Ishikura, Y. Kato, T. Ooyanagi and M. Miyauchi: IEEE J. Lightwave Technol. **7** (1989) 577.
29) S. T. Davey, D. L. Williams, B. J. Ainslie, W. J. M. Rothwell and B. Wakefield: IEE Proc. J. **136** (1989) 301.
30) D. M. Spirit, L. C. Blank, S. T. Davey and D. L. Williams: IEE Proc. J. **4** (1990) 221.
31) K. X. Liu and E. Garmire: IEEE J. Quantum Electron. **27** (1991) 1022.
32) A. Uchida, M. Takeoka, T. Nakata and F. Kannari: IEEE J. Lightwave. Technol. **16** (1998) 92.
33) P. Urquhart: IEE Proc. **135** (1988) 385.
34) E. M. Dianov, M. V. Grekov, I. A. Bufetov, S. A. Vasiliev, O. I. Medvedkov, V. G. Plotnichenko, V. V. Koltashev, A. V. Belov, M. M. Bubnov, S. L. Semyonov and A. M. Porkhorov: Electron. Lett. **33** (1997) 1542.
35) S. V. Chernikov, N. S. Platonov, D. V. Gapontsev, D. I. Chang, M. J. Guy and J. R. Taylor: Electron. Lett. **34** (1998) 680.
36) V. I. Karpov, E. M. Dianov, V. M. Paramonov, O. I. Medvedkov, M. M. Bubnov, S. L. Semyonov, S. A. Vasiliev, V. N. Protopopov, O. N. Egorova, V. F. Hopin, A. N. Guryanov, M. P. Bachynski and W. R. L. Clements: Opt. Lett. **24** (1999) 887.
37) A. Bertoni: Opt. Quantum Electron. **29** (1997) 1047.
38) S. R. Chinn: Electron. Lett. **33** (1997) 607.
39) A. Bertoni and G. C. Reali: Appl. Phys. B **67** (1998) 5.
40) G. Vareille, O. Audouin and E. Desurvire: Electron. Lett. **34** (1998) 675.